Materials Advances

ROYAL SOCIETY OF CHEMISTRY

PAPER

View Article Online
View Journal | View Issue

Cite this: *Mater. Adv.*, 2024, 5, 4401

Integrating the amino-functionalized MOF-5 film with the silver nanoparticle substrate for a high SERS enhancement effect and long-term stability

Nguyen La Ngoc Tran, [abc] Le Hong Tho,[abc] Ngoc Quang Tran, [bc] Hanh Kieu Thi Ta,[abc] Bach Thang Phan, [bc] Nguyet N. T. Pham, [bd] Tan Le Hoang Doan *[bc] and Nhu Hoa Thi Tran *[ab]

Plasmonic has sparked a lot of interest in customizing localized surface plasmon resonance for new biosensing approaches. We report experimental results that highlight the mechanisms underpinning the combined electromagnetic and chemical contributions of surface-enhanced Raman scattering. The amino-functionalized metal–organic framework-5 (MOF-5-NH_2) platforms were demonstrated to have the ability to enhance Raman scattering through sensitivity with molecular Raman probes such as rhodamine B (RhB) and methylene blue (MB). This multi-component substrate allows for the detection of molecules at low concentrations as low as 1.78×10^{-10} M of MB and 1.26×10^{-12} M of RhB, with the following durability and stability SERS signals after 120 days of storage. The plasmon excitations of the double-layer substrates caused a resonant increase in Raman scattering, recording an approximately 13-fold increase in signal amplification after the deposition of a 3D structure layer on the silver single-membrane substrate. The location of the porous outer layer on the plasmonic surface increases the *in situ* molecular density, reducing the distance between the SERS-active region and the molecules responsible for molecule manipulation near hotspot engineering. Our findings provide a general framework for investigating the contribution of metal nanomaterials (NPs) and metal–organic frameworks to SERS, as well as for improving the Raman efficiency of Ag NP templates through deposition modification using MOF-5-NH_2 films. This innovative approach paves the way for SERS platforms on ultrasensitive substrates and biosensing applications.

Received 30th January 2024,
Accepted 1st April 2024

DOI: 10.1039/d4ma00087k

rsc.li/materials-advances

1. Introduction

Surface-enhanced Raman scattering (SERS) is a vibrational spectroscopic technique that uses molecular fingerprints and is a promising nondestructive testing technology. Thus, the great potential of SERS sensing for hazardous molecule detection is highly sensitive, quick, and accurate because of its low susceptibility to environmental interference during *in situ* detection.[1] SERS is a Raman spectroscopy-based analytical method that uses in-material binding and light interaction to identify drugs and biosensors.[2,3] Metal-based nanoparticles have been used in a wide range of industries, including bioengineering, photocatalysis, energy, photo electronics, and sensors,[4] with gold/silver materials being the most commonly used to generate SERS phenomena. Based on the "hot spots" produced by homogenized noble-metal nanoparticle substrate, the low detection limit and high sensitivity can be increased from 10^2 to 10^{14} times over conventional Raman scattering.[5] Due to the limitations of metallic materials when used alone, such as low repeatability and stability, they are often conjugated or coupled to other nanostructured materials to achieve their use as SERS probes. Because of their exceptional optical, antimicrobial, and plasmonic capabilities, Ag nanoparticles (Ag NPs) have drawn considerable interest.[6] Optical properties of Ag NPs depend on their shape and size due to an electron cloud having varied energies.[7]

SERS substrates normally on gold or silver colloids are quickly impacted by interference, restricting SERS technology's use and advancement in direct detection.[8,9] This challenge necessitates the search for alternate substrates with good sensitivity, selectivity, and stability for sample detection without further dilution or pretreatment. Various alternative materials used as SERS substrates, such as activated carbon,

[a] *Faculty of Materials Science and Technology, University of Science, Ho Chi Minh City, Vietnam. E-mail: ttnhoa@hcmus.edu.vn*
[b] *Vietnam National University, Ho Chi Minh City, Vietnam*
[c] *Center for Innovative Materials and Architectures (INOMAR), HoChiMinh City, Vietnam. E-mail: dlhtan@inomar.edu.vn*
[d] *Faculty of Chemistry, University of Science, Ho Chi Minh City, Vietnam*

hyperbolic metamaterials, and flexible polymers such as polydimethylsiloxane, have improved the limited stability of metal nanoparticles.[10,11] Therefore, a more efficient substrate platform for boosting sensitivity and intensifying SERS from Ag NPs is necessary.

Metal–organic frameworks (MOFs) have sparked a lot of attention due to their ability to efficiently trap organic molecules, resulting in considerably increased stability and excellent activity retention.[12–15] Because of their remarkable porosity performance and huge specific surface area, MOFs have been widely used in separation,[16] catalysis,[17] and other applications since their discovery.[18,19] MOFs and SERS technology combination have significantly increased the detection limit and response time of typical SERS substrates.[20,21] MOF-coated Ag NPs may retain high SERS activity in biological analyses, improving the detection efficiency of SERS sensors.[22] Nevertheless, the MOFs used in such sensors are often synthesized using hydrothermal techniques, which have the disadvantages of a long fabrication time and nonuniformity.[23] Chemical deposition provides the advantages of low time cost, *in situ* growth on material surfaces, and more adjustable shape and thickness.[24,25] However, the use of a programmable chemical self-assembly MOF layer on the SERS sensor substrate for constructing a highly selective, sensitive, and repeatable sensor for the detection of organic dye has not yet been studied.

Methylene blue (MB) is a common dye that is very poisonous and carcinogenic to mammals; hence, MB in water sources causes serious harm to human health and the ecological environment.[26,27] Rhodamine B (RhB) is a type of basic dye that is detrimental to human health. It is easy to add illegally to meals as a colorant because it is cheap and abundant. Spectrophotometry,[28,29] electrochemical detection,[30,31] high-performance liquid chromatography,[32,33] immunochromatography assay, and enzyme-linked immunosorbent assay[34] are all methods for detecting trace RhB. Although the methods described above have numerous advantages, they nevertheless necessitate a complex separation procedure, sophisticated instrumentation, and lengthy detection time. In comparison to the preceding approaches, SERS detection of the target is easy, quick, sensitive, and non-destructive, gradually capturing people's attention.[35]

In this study, amino-functionalized MOF-5 (MOF-5-NH_2) coated silver nanoparticles were produced, and their suitability as SERS probes for detecting dye solutions was proven. The MOF-5-NH_2, whose structure is composed of six-connected octahedral Zn_4O clusters and amine-functionalized terephthalate linkers (H_2BDC-NH_2),[36] is prepared at room temperature for a short time. Based on its advantage, MOF-5-NH2 has functional groups in the organic linker configuration (H2BDC-NH2) as active free radicals, which quickly and directly attach Ag NPs *via* bridge amino linkers. The amino-functional groups of MOF-5 frameworks provide a quick interaction for Ag NPs, leading to MOF-5-NH_2 self-assembling on the surface of the Ag NP substrate to obtain the Ag NPs/MOF-$_5$-NH2 double-layer by utilizing a chemical process. The SERS sensor chips were then built by layering Ag NPs/MOF-5-NH_2 on glass slides, allowing for the detection of dye solutions *via* the interaction of the SERS-active area with the target molecules. The SERS intensity of RhB at different Raman shifts exhibits a linear relationship with the logarithm of RhB concentration ranging from 10^{-6} to 10^{-11} M at the excitation wavelength of 532 nm, and the detection limit can reach 1.26×10^{-12} M. Subsequently, the Ag NPs/MOF-5-NH_2 double-layer was used to detect the MB dye in aqueous solution, revealing that the limit of detection was low, down to 1.78×10^{-10} M, and the enhance Raman attained 1.42×10^{9}. Investigations were also conducted into the different analytical properties of the double-layer-based SERS chip, such as its long-term stability, repeatability, and uniformity.

2. Materials and methods

2.1 Materials

Chemicals purchased from Sigma-Aldrich (Co., MO, USA) include silver nitrate, ethylene glycol, sodium sulfide nonahydrate, zinc acetate, amino terephthalic acid, cetyltrimethylammonium bromide, polyvinylpyrrolidone, *N*,*N*-dimethylformamide, (3-aminopropyl)triethoxysilane (APTES), rhodamine B, methylene blue, sodium hydroxide, and ethanol with a purity of 99%. We used microscope glass slides manufactured by ISOLAB Laborgeräte GmbH, Eschau, Germany, which consist of chemical compositions such as SiO_2 (75 ± 5 wt %), Na_2O (15 ± 2 wt %), CaO, and MgO (10 ± 2 wt %).

2.2 Fabrication of the double-layer structure as SERS substrates

Immersion and ultrasonication in 0.5 M sodium hydroxide solution for 10 minutes resulted in clean surface glass slides. The surface glass was then treated with deionized water,

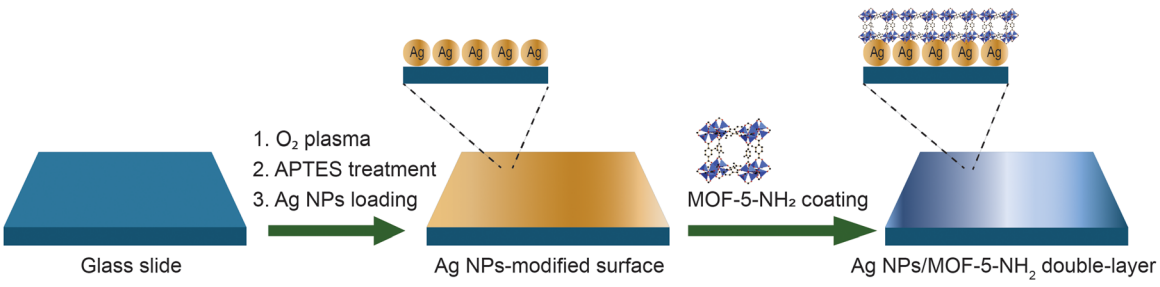

Scheme 1 Illustration of the Ag NPs/MOF-5-NH_2 double-layer fabricated process.

acetone, and ethanol by ultrasonic for 10 minutes per round. An oxygen plasma machine (CUTE-1MPR, Femto Science Inc., Korea) was used to alter and functionalize the surface hydroxyl groups (–OH) for 2 minutes. The glass slides were treated with 3% APTES to generate an amino group ($–NH_2$) by soaking the sample in the solution for 2 hours. The chemical approach was used to assemble the coated film layer by layer (Scheme 1). The MOF-5-NH_2 was synthesized by modifying a previously reported method.[37] Silver nanoparticles were synthesized from the reduction of silver nitrate by sodium sulfide nonahydrate in an ethylene glycol solution, and details of the procedure are presented in our publication.[25] A high electrostatic force from the substrate's functional group immobilized Ag NPs for 2 hours before immersing them in MOF-5-NH_2 solution for three days at room temperature, yielding an Ag NP/MOF-5-NH_2 double-layer structure.

2.3 Characterization

We utilize instruments to investigate the characterized properties of materials, including a powder X-ray diffraction machine (PXRD, Bruker D8 Advance diffractometer, λ = 1.54178 Å), UV-visible spectroscopy (V-770 visible/NIR, JASCO, Tokyo, Japan), and field emission scanning electron microscope (FESEM, Hitachi S4800, USA), with energy dispersive X-ray (EDX) spectroscopy. The analyte's Raman spectra were recorded using micro-Raman spectroscopy (Horiba Xplora One, Horiba Scientific, Horiba Ltd), employing illumination through a green laser with a wavelength of 532 nm, a 25 mW power source, a 10× objective microscope, and a 10 s accumulation time.

2.4 Simulation methods

The finite-difference time-domain (FDTD) calculation was performed using a code of FDTD solutions developed by Lumerical Solutions to accurately calculate the dispersion of a composite material by solving Maxwell equations. Taking advantage of this, we demonstrate the electric field distribution on the surface of the Ag NPs compared to that of Ag NPs/MOF-5-NH_2. We hypothesize that the polarization of the materials occurs solely in the directions corresponding to the wave vector **k** of the 532-nm laser. The transversal component of k is perpendicular to the plane of the Ag NPs/MOF-5-NH_2 double-layer on the glass substrate. For relevance to the experimental observation of the SERS analysis, the structural parameters of the Ag NPs and MOF-5-NH_2 were set to be the same as those of the experiment. The spherical Ag NPs with a diameter of 54 nm were designed to be underneath the 80 nm length of cubic MOF-5-NH_2 in the double-layer structure. The distance between the two layers of Ag NPs and MOF-5-NH_2 was 2 nm, equaling the constructed gap among the Ag NPs for the best electric field enhancement.[38] For comparison, a similar set was applied to the sole Ag NPs without the presence of MOF-5-NH_2. The total-field scattered-field source mode perfectly matched layer (PML) boundary conditions and refractive indices for MOF-5-NH_2[39] and Ag NPs[40] were selected and built up. Additionally, the chosen mesh size in the FDTD calculation domains was 1 nm^2 for every 3D plane with a minimum mesh step and an auto-shutoff value of 0.25 nm and 10^{-5}, respectively.

3. Results and discussion

3.1 Characterization of the Ag NP/MOF-5-NH_2 double-layer

The Ag NP solution was subjected to UV-vis absorption spectra, and as shown in Fig. 1a, the localized surface plasmon resonance action caused the absorption peak of Ag to appear near 406 nm.[41] The surface plasmon resonance band gradually moves to longer wavelengths and becomes wider as the covering density of Ag nanoparticles increases. As a result of the Ag nanoparticle plasmonic interaction, which produces a distinct plasmon resonance mode, a very broad band that spans the UV to IR area appears. By reacting with APTES solution, these hydroxy-functionalized glass slides were embellished with amine groups to produce an Ag NP membrane as the initial platform and then through the Ag NP surface to quickly react with the amine groups on MOF-5-NH_2 to build a double-layer on the substrate. Four diffraction peaks at 2 of 38.2°, 44.3°, 64.4°, and 77.8° were in accordance with the (111), (200), (220), and (311) crystalline planes of silver,[42,43] respectively, in the XRD patterns of the silver film (Fig. 1b). These studied peaks demonstrated that silver nanoparticles were smoothly synthesized using the reduction process and showed the emergence of a face-centered cubic silver phase.[25,44] Fig. 1c, a typical FESEM image, clearly shows that Ag NPs have a spherical morphology, a uniform size distribution, and an average diameter of 54 ± 5 nm. The Ag NPs are depicted in Fig. 1d, with HRTEM pictures being homogeneous in size and sphere-shaped, measuring 56 nm in diameter.

It is reported that MOF-5-NH_2 has a broad absorption zone with an excitation wavelength ranging from 300 to 400 nm (Fig. 2a).[45] The -COOH group on the surface of MOF-5-NH_2 and the benzenoid band of the n–π* transitions of MOF-5-NH_2 are responsible for the observed absorption peak at 367 nm.[46,47] XRD was used to characterize the crystal structures of the Ag

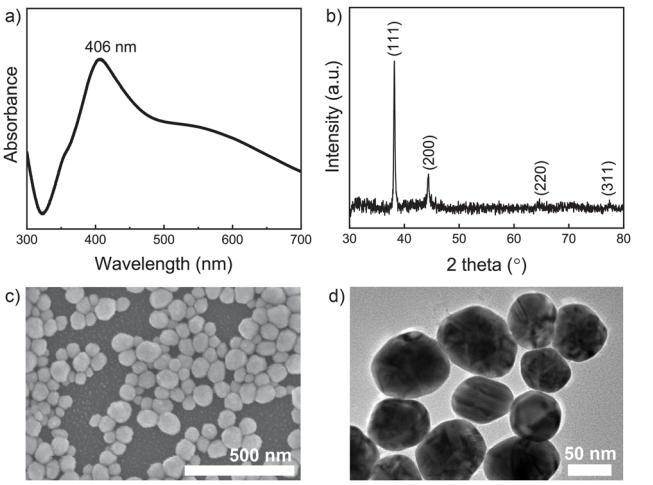

Fig. 1 (a) UV-vis absorption spectra, (b) XRD patterns, (c) FESEM, and (d) HRTEM images of Ag NPs.

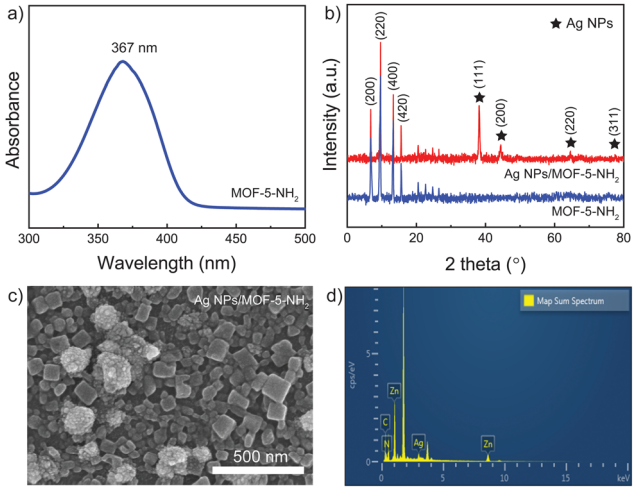

Fig. 2 (a) UV-vis absorption spectra of MOF-5-NH_2. (b) XRD patterns, (c) FESEM images, and (d) EDX analysis of Ag NP/MOF-5-NH_2 double-layer.

NPs/MOF-5-NH_2 double-layer, and the findings are shown in Fig. 2b. Strong diffraction major peaks corresponding to the (200), (220), (400), and (420) planes can be observed in the XRD patterns of MOF-5-NH_2.[48,49] Many additional peaks with 2θ at 38.1°, 44.2°, 64.4°, and 77.3°, which can be indexed to the (111), (200), (220), and (311) planes of the face-centered cubic phase of silver,[50] indicate that MOF-5-NH_2 was successfully deposited on the surface of Ag NP-coating substrate. Crystals of MOF-5-NH_2 were successfully localized above the Ag NP platform, as shown by the representative FESEM image of the double-layer structure (Fig. 2c). By containing a large number of amine groups, MOF-5-NH_2 can interact easily with Ag NP surfaces by ion pairing, facilitating the uniform development of the self-assembly layer. The elemental compositions of these samples were tested by EDX analysis to verify the component surface (Fig. 2d). Ag NP/MOF-5-NH_2 double-layer assembly is demonstrated by the presence of an Ag, Zn, C, and O-containing double-layer substrate.

3.2 SERS-enhance ability of the Ag NP/MOF-5-NH2 double-layer

We analyzed the Raman spectrum of RhB recorded by the SERS substrate to evaluate the improved performance of the sensor chip. Because RhB has a fluorescence effect,[51] using a long-wave laser can eliminate fluorescence interference; nevertheless, using a long-wave laser appears to have a heating effect, and high power is not recommended. Because light scattering strength is inversely related to fourth wavelength power, a short wavelength laser can provide more vigorous Raman intensity and higher sensitivity. We used 10^{-9} M of RhB and 10^{-6} M of MB as probe molecules to determine the proportional contribution of the MOF-5-NH_2 layer to the SERS effect. In Fig. 3a, all the distinctive Raman shifts of RhB appeared in full, with the peak intensity recorded by the Ag NP/MOF-5-NH_2 double-layer substrate being 13 times greater than that of the initial platform. The most characteristic peaks are situated at 1648 cm^{-1}

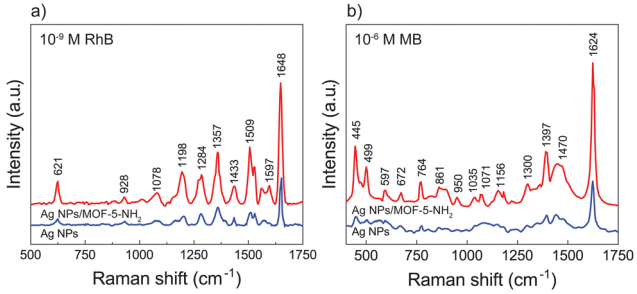

Fig. 3 Compare differences in Raman intensity of initial platform and double-layer substrates through the detection ability for (a) 10^{-9} M of RhB và (b) 10^{-6} M of MB.

(C–C, C═C), 1597 cm^{-1} (C═N), 1507 cm^{-1} (C–H), 1433 cm^{-1} (C–C, C═C–C), 1357 cm^{-1} (C–C), 1284 cm^{-1} (H–C–H), 1198 cm^{-1} and 1078 cm^{-1} (C–H), 928 cm^{-1} and 621 cm^{-1} (C–C–C), with detailed peak affiliation shown in Table 1.[52,53] Even though a SERS signal of 10^{-6} M of MB was detected by two structures, the Raman intensity was recorded by a double-layer much higher than that of the Ag NP substrate, as shown in Fig. 3b. Notably, the primary distinctive peaks of MB at 455 cm^{-1} and 499 cm^{-1} are assigned to C–N–C and C–S–C skeletal deformation vibrations, respectively.[54,55] The bands at 1397 cm^{-1} and 1624 cm^{-1} correspond to C–N and C–C ring stretching modes, respectively.[55,56] In conclusion, it can be stated that the MOF-5-NH_2 layer directly influenced SERS detection performance due to its chemical mechanism-enhancing contribution. MOF-5-NH_2 successfully adsorbs target molecules and improves the analytical signal due to its unique porous structure and excellent dispersibility.[13,57]

Fig. 4a and c shows the Raman spectra acquired for the Ag NP/MOF-5-NH_2 double-layer substrate while sensing various dye solution concentrations. With an increase in concentration, the Raman intensities of RhB and MB tended to increase. The Raman signal was also discernible at low concentrations, and the change in Raman strength at varied dye concentrations was plotted. Fig. 4b and d also shows the correlation curve between the logarithm of the dye concentration and various Raman signals obtained (with the highest regression coefficient, R^2 averages above 0.98), demonstrating that this SERS method can be used to quantify molecules. The concentrations of RhB and MB showed a good linear relationship ranging from 10^{-6} to 10^{-11} M and 10^{-4} to 10^{-9} M, with a detection limit of 1.26 × 10^{-12} M for RhB and 1.78 × 10^{-10} M for MB, respectively. The change in the relative strength of characteristic spectral characteristics is caused by analyte-surface interaction, which is influenced by adsorption sites, adsorption orientation, and the

Table 1 Limit of detection (LOD) and EF comparison of SERS active for the other substrates

	Rhodamine B		Methylene blue	
SERS substrate	LOD (M)	EF	LOD (M)	EF
Ag@SiO_2-Au NPs[62]	5 × 10^{-9}	1.5 × 10^4		
$CoTiO_3$@Ag NPs[63]	10^{-9}	1.44 × 10^5		
GO-TiO_2[64]			6 × 10^{-7}	5 × 10^4

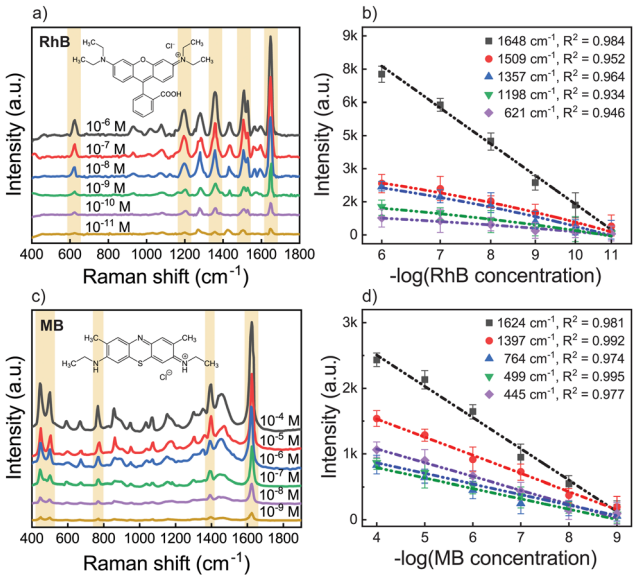

Fig. 4 SERS spectra and calibration plot of the Raman intensity of (a) and (b) RhB and (c) and (d) MB with various concentrations and of Ag NP/MOF-5-NH_2 double-layer.

vibrational modes of the adsorbed molecule on the active metal surface. The porous structure of the proposed MOF-5-NH_2 serves as a reactor, concentrating chiral target molecules into the nanopores of Ag NPs.[12,58,59]

The enhancement factor (EF) for SERS calculation is intuitive for analytical chemistry applications in terms of more signals that can be expected from SERS under experimental conditions compared to standard Raman. To indicate the SERS sensitivity of the Ag NP/MOF-5-NH_2 double-layer, we chose the Raman shift at 1648 cm^{-1} of RhB and 1624 cm^{-1} of MB to determine EF, which was calculated according to the formula in detail.[60,61] The typical EF of RhB was 2.89×10^{11} while that of MB was 1.42×10^{9} in this study. This result revealed that the created Ag NP/MOF-5-NH_2 chip had improved SERS efficiency, which might be related to the uniform distribution of the Ag NP-electromagnetic field with support chemical enhancement by the matrix frame of the amino-functionalized MOF-5. The above results indicated that Ag NPs/MOF-5-NH_2 double-layer substrate had high SERS performance with good enhanced effect and ability of limit detection at low target concentration when compared with other platforms,[62–65] as shown in Table 1.

3.3 Uniformity and long-term stability of SERS double-layer

To confirm the reproducibility of the Ag NPs/MOF-5-NH_2 double-layer structure, we randomly selected 12 test sites on the SERS substrate with the intensity of most areas being uniform. Fig. 5a depicts the SERS mapping image and the SERS signal intensity distribution of 1624 cm^{-1}. Even at low concentrations, MB signals can be identified (Fig. 5a), showing that the Ag NP/MOF-5-NH_2 structure has great sensitivity for SERS investigation due to its 3D plasmonic matrix. The SERS spectra of MB with a concentration of 10^{-6} M showed highly consistent and completely distinctive peaks at all collected concentrations, as shown in Fig. 5b. Because the band at 1624 cm^{-1} is dependent on LSPR, it was used to calculate the relative standard deviation (RSD), which from the 1624 cm^{-1} peaks was 3.8% (Fig. 5c). The results demonstrated that the substrate exhibited good LSPR-enhanced signal repeatability and homogeneity.

SERS spectra of RhB (10^{-7} M) were measured throughout time to study the long-term stability of manufactured Ag NPs/MOF-5-NH_2 chips (Fig. 6a) because the long-term stability is another key index for assessing the performance of SERS substrates. After 120 days of air exposure, all SERS intensities of RhB were slowly lowered, in which the SERS intensity obtained from the typical Raman shift of 1648 cm^{-1} is still above 70% after 60 days and as low as 48%. This demonstrates the outstanding long-term stability of the prepared Ag NPs/MOF-5-NH_2 double-layer chips. However, the efficient pre-concentration effect of MOF-5-NH_2 may contribute to improving the stability of target molecules adhered to the chip as well as protection from the MOF coating layer before the influence of the environment, which causes oxidation of the Ag NP platform and rapidly reduces SERS-performance.[66,67] Raman spectrum of RhB (10^{-6} M) was recorded from 14 random places after 120 days on Ag NP/MOF-5-NH_2 double-layer devices, as shown in Fig. 6b. As an outcome, the Ag NP/MOF-5-NH_2 structure has excellent reproducibility and repeatability in long-term storage compared to other Ag NP substrates.[25]

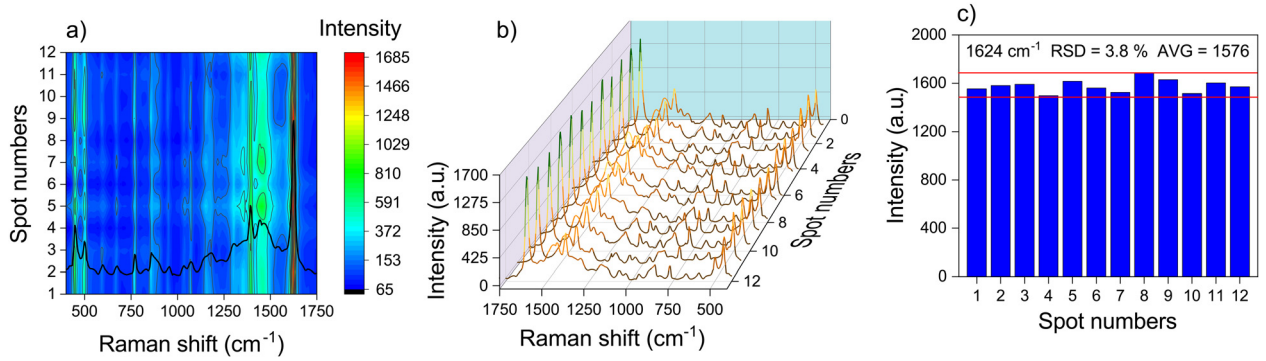

Fig. 5 (a) and (b) SERS spectra from 10^{-6} M of MB collected randomly from 12 plots and (c) the corresponding column diagram of the intensity SERS was recorded by Ag NP/MOF-5-NH_2 double-layer.

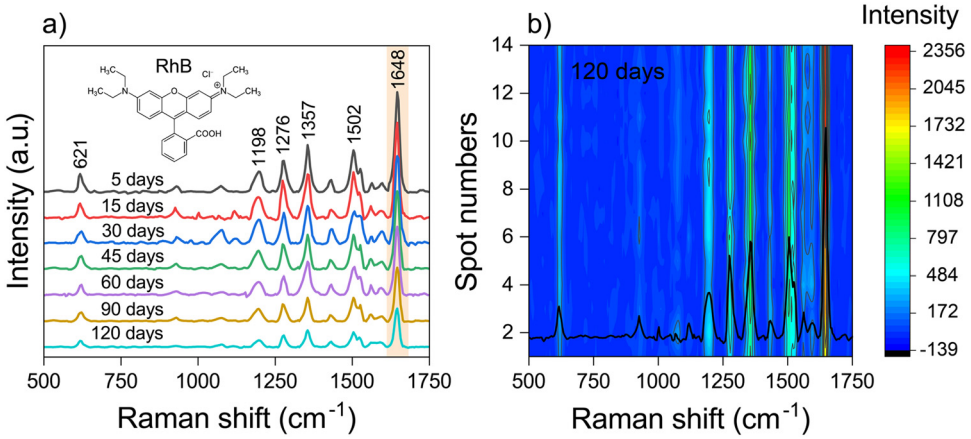

Fig. 6 (a) SERS spectra and (b) mapping of SERS spectra from 10^{-7} M of RhB collected randomly from 14 plots after 120 days of storage.

3.4 FDTD calculation

To prove the high SERS enhancement effect of the Ag NP/MOF-5-NH_2 double-layer structure, FDTD calculation on the local electromagnetic fields was demonstrated *via* 2D photographs. The "hot spots" are clearly demonstrated in the 2 nm gap between the adjacent Ag NPs shown in Fig. 7a and b. In response to the excitation of the 532-nm laser, the electric field over the Ag NP surface appears as a dipole-liked shape due to the polarization.[68] The highest norm is observed in the "hot spots" region with a value of 3.72 times greater than that of the incident beam, which agrees with other studies.[40,69] Furthermore, the electric field is particularly strong in the space between the two surfaces due to the existence of an 80 nm cubic length MOF-5-NH_2. Additionally, the magnitude of the local electric fields in the vicinity of Ag NPs/MOF-5-NH_2 is 5.59 times that of the origin, which is slightly higher than that observed in Fig. 7a. This contributes to elucidating the recent hypothesis on the MOF-5-NH_2 support for SERS signal enhancement generally. The pore holes of MOF-5-NH_2 nanostructures naturally increase the probability of analyte absorption approaching close to the "hot spots" and the interface between Ag NPs and MOF-5-NH_2, where the strongest electric field distribution occurs.[70,71] The FDTD simulation results well elucidated the high sensitivity of the experimental SERS detection of MB and RhB on the Ag NPs/MOF-5-NH_2 substrate in this study.

4. Conclusions

In conclusion, the Ag NP/MOF-5-NH_2 double-layer platform is easily synthesized using the self-assembly deposition approach. The MOF-5-NH_2 has the potential to improve effective chemical mechanism sensing, and its advantages include molecular capture ability, improved sensitivity, and stability. Therefore, the SERS substrate based on MOFs provides simultaneous activation of both electromagnetic and chemical effects. The MOF-5-NH_2 layer outside as 3D frameworks was supported for the standard Ag NP layer, including enhanced storage stability, protection, and, most crucially, the ability to be absorbed by targets in the SERS-active region. This article will explore another use of MOFs in conjunction with plasmonic materials, paving the way for the design and manufacture of high-performance sensors. Furthermore, it is necessary to focus research on various composite structures to combine the

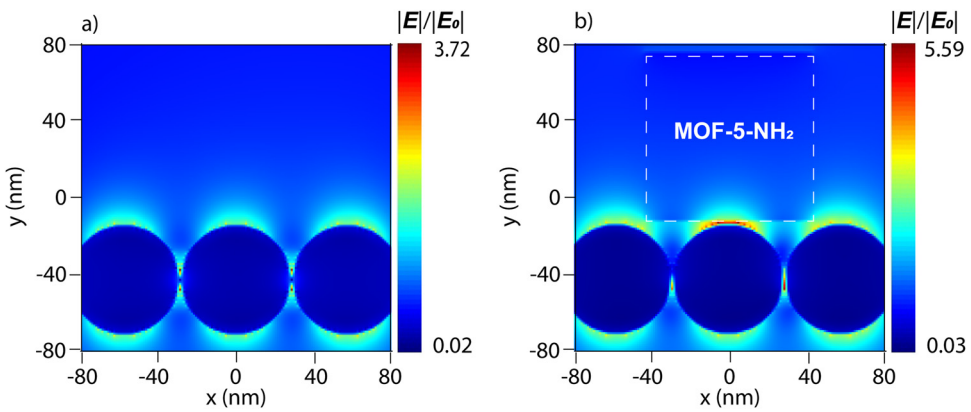

Fig. 7 FDTD simulation of electric field distribution on the surface of (a) Ag NPs of 54 nm diameter and (b) Ag NPs/MOF-5-NH_2 double-layer structure. The color bar varies on a logarithmic scale.

unique properties of different materials. The developed SERS platform on other types of substrates expands their flexibility compared to the glass used for practical applications.

Author contributions

The manuscript was written through the contributions of all authors. All authors have approved the final version of the manuscript.

Conflicts of interest

There are no conflicts to declare.

Acknowledgements

This research is funded by Vietnam National University, Ho Chi Minh City (VNU-HCM) under grant number A2023-50-01.

References

1 M. Arabi, A. Ostovan, Z. Zhang, Y. Wang, R. Mei, L. Fu, X. Wang, J. Ma and L. Chen, *Biosens. Bioelectron.*, 2021, **174**, 112825.
2 H. Fisk, C. Westley, N. J. Turner and R. Goodacre, *J. Raman Spectrosc.*, 2016, **47**, 59–66.
3 X. X. Han, R. S. Rodriguez, C. L. Haynes, Y. Ozaki and B. Zhao, *Nat. Rev. Methods Primers*, 2022, **1**, 1–17.
4 J. Chen, B. Lim, E. P. Lee and Y. Xia, *Nano Today*, 2009, **4**, 81–95.
5 T. Li, Y. Shen, H. Chen, Y. Xu, D. Wang, F. Cui, Y. Han and J. Li, *Foods*, 2021, **10**, 2385.
6 G. V. P. Kumar, S. Shruthi, B. Vibha, B. A. A. Reddy, T. K. Kundu and C. Narayana, *J. Phys. Chem. C*, 2007, **111**, 4388–4392.
7 M. Kahraman, Ö. Aydin and M. Çulha, *ChemPhysChem*, 2009, **10**, 537–542.
8 Q. Zhang, D. Li, X. Cao, H. Gu and W. Deng, *Anal. Chem.*, 2019, **91**, 11192–11199.
9 N. L. N. Tran, T. A. Nguyen, T. L. H. Doan, H. V. T. Nguyen, V. T. Huong, T. T. Van Tran, H. Ju, T. H. Huy, H. Van Le and N. H. T. Tran, *ChemNanoMat*, 2023, **9**, e202300164.
10 Y. U. Guo, J. Yu, C. Li, Z. Li, J. Pan, A. Liu, B. Man, T. Wu, X. Xiu and C. Zhang, *Opt. Express*, 2018, **26**(17), 21784–21796.
11 C. Zheng, L. Zhang, F. Wang, Y. Cai, S. Du and Z. Zhang, *Talanta*, 2018, **188**, 630–636.
12 H. Lai, G. Li, F. Xu and Z. Zhang, *J. Mater. Chem. C*, 2020, **8**, 2952–2963.
13 W. P. Lustig, S. Mukherjee, N. D. Rudd, A. V. Desai, J. Li and S. K. Ghosh, *Chem. Soc. Rev.*, 2017, **46**, 3242–3285.
14 M. Chang, J. Ren, Y. Wei, J. X. Wang, Q. Yang, D. Liu and J. F. Chen, *Sep. Purif. Technol.*, 2021, **279**, 119656.
15 C. Healy, K. M. Patil, B. H. Wilson, L. Hermanspahn, N. C. Harvey-Reid, B. I. Howard, C. Kleinjan, J. Kolien, F. Payet, S. G. Telfer, P. E. Kruger and T. D. Bennett, *Coord. Chem. Rev.*, 2020, **419**, 213388.
16 H. L. Nguyen, R. Matheu, C. S. Diercks, T. L. H. Doan, B. T. Nguyen and K. E. Cordova, *ACS Mater. Lett.*, 2022, **4**, 2375–2380.
17 M. H. D. Dang, T. T. T. Nguyen, B. Q. G. Le, L. H. T. Nguyen, N. X. D. Mai, M. Van Nguyen, P. H. Tran and T. L. H. Doan, *J. Ind. Eng. Chem.*, 2022, **111**, 111–120.
18 B. Q. G. Le and T. L. H. Doan, *Wiley Interdiscip. Rev.: Nanomed. Nanobiotechnol.*, 2023, **15**, e1874.
19 K. Y. Shin, L. H. T. Nguyen, H. L. Nguyen, A. Mirzaei, V. N. H. Tran, N. X. D. Mai, N. Q. Tran, W. Oum, E. B. Kim, H. M. Kim, T. B. Phan, T. L. H. Doan, S. S. Kim and H. W. Kim, *Sens. Actuators, B*, 2023, **394**, 134425.
20 L. Jiang, C. H. He, H. Y. Chen, C. Y. Xi, E. K. Fodjo, Z. R. Zhou, R. C. Qian, D. W. Li and M. E. Hafez, *Anal. Chem.*, 2021, **93**, 12609–12616.
21 M. Lafuente, S. De Marchi, M. Urbiztondo, I. Pastoriza-Santos, I. Pérez-Juste, J. Santamaría, R. Mallada and M. Pina, *ACS Sens.*, 2021, **6**, 2241–2251.
22 Q. Q. Chen, R. N. Hou, Y. Z. Zhu, X. T. Wang, H. Zhang, Y. J. Zhang, L. Zhang, Z. Q. Tian and J. F. Li, *Anal. Chem.*, 2021, **93**, 7188–7195.
23 J. L. Hauser, M. Tso, K. Fitchmun and S. R. J. Oliver, *Cryst. Growth Des.*, 2019, **19**, 2358–2365.
24 N. Tran Truc Phuong, T. Xoan Hoang, N. La Ngoc Tran, L. Gia Phuc, V.-D. Phung, H. Kieu Thi Ta, T. Ngoc Bach, N. Hoa Thi Tran and K. The Loan Trinh, *Spectrochim. Acta, Part A*, 2021, **263**, 120179.
25 N. T. Truc Phuong, V. Q. Dang, L. Van Hieu, T. N. Bach, B. X. Khuyen, H. K. Thi Ta, H. Ju, B. T. Phan and N. H. Thi Tran, *RSC Adv.*, 2022, **12**, 31352–31362.
26 P. O. Oladoye, T. O. Ajiboye, E. O. Omotola and O. J. Oyewola, *Results Eng.*, 2022, **16**, 100678.
27 I. Khan, K. Saeed, I. Zekker, B. Zhang, A. H. Hendi, A. Ahmad, S. Ahmad, N. Zada, H. Ahmad, L. A. Shah, T. Shah and I. Khan, *Water*, 2022, **14**, 242.
28 R. Ji, Z. Zhao, X. Yu and M. Chen, *Optik*, 2019, **181**, 796–801.
29 Y. Li, Y. Lu, X. Jia, C. Zeng, Y. Hu, J. Liang, Y. Li, J. Zhang, Z. Xie, N. Zhang, X. Yu, Y. Xu, J. Lu, L. Tang, J. Xia and G. Yang, *IOP Conf. Ser.: Earth Environ. Sci.*, 2019, **376**, 012043.
30 S. Feng, W. Ding, Y. Zhang, J. Wu, Z. Zou, T. Wu and Q. Tang, *J. Solid State Chem.*, 2021, **303**, 122508.
31 Q. He, J. Liu, Y. Tian, Y. Wu, F. Magesa, P. Deng and G. Li, *Nanomaterials*, 2019, **9**, 958.
32 H. İ. Ulusoy, *Colloids Surf., A*, 2017, **513**, 110–116.
33 P. Tao, Y. Xu, C. Song, Y. Yin, Z. Yang, S. Wen, S. Wang, H. Liu, S. Li, C. Li, T. Wang and M. Shao, *Sep. Purif. Technol.*, 2017, **179**, 175–183.
34 M. Oplatowska and C. T. Elliott, *Analyst*, 2011, **136**, 2403–2410.
35 H. Wang, X. Guo, S. Fu, T. Yang, Y. Wen and H. Yang, *Food Chem.*, 2015, **188**, 137–142.
36 Y. T. Dang, M. H. D. Dang, N. X. D. Mai, L. H. T. Nguyen, T. B. Phan, H. V. Le and T. L. H. Doan, *J. Sci.: Adv. Mater. Devices*, 2020, **5**, 560–565.

37 N. La Ngoc Tran, B. T. Phan, H. K. T. Ta, T. T. K. Chi, B. T. T. Hien, N. T. T. Phuong, C. C. Nguyen, T. L. H. Doan and N. H. T. Tran, *Sens. Actuators, A*, 2022, **347**, 0924–4247.
38 R. X. He, R. Liang, P. Peng and Y. N. Zhou, *J. Nanopart. Res.*, 2017, **19**, 267.
39 L. M. Yang, E. Ganz, S. Wang, X. J. Li and T. Frauenheim, *J. Mater. Chem. C*, 2015, **3**, 2244–2254.
40 A. Y. Zyubin, I. I. Kon, D. A. Poltorabatko and I. G. Samusev, *Nanomaterials*, 2023, **13**, 897.
41 Y. Zhao, J. Shao, Z. Jin, W. Zheng, J. Yao and W. Ma, *Food Chem.*, 2023, **412**, 135526.
42 K. Girel, A. Burko, A. Barysiuk, S. Dubkov, D. Gromov and H. Bandarenka, *Curr. Appl. Phys.*, 2023, **49**, 18–24.
43 B. Park, T. V. Dang, J. Yoo, T. D. Tran, S. M. Ghoreishian, G. H. Lee, M. Il Kim and Y. S. Huh, *Sens. Actuators, B*, 2022, **369**, 132246.
44 Z. Leng, D. Wu, Q. Yang, S. Zeng and W. Xia, *Optik*, 2018, **154**, 33–40.
45 J. G. Nguyen, K. K. Tanabe and S. M. Cohen, *CrystEngComm*, 2010, **12**, 2335–2338.
46 A. R. Chowdhuri, T. Singh, S. K. Ghosh and S. K. Sahu, *ACS Appl. Mater. Interfaces*, 2016, **8**, 16573–16583.
47 V. Nanduri, I. B. Sorokulova, A. M. Samoylov, A. L. Simonian, V. A. Petrenko and V. Vodyanoy, *Biosens. Bioelectron.*, 2007, **22**, 986–992.
48 H. Zhao, H. Song and L. Chou, *Inorg. Chem. Commun.*, 2012, **15**, 261–265.
49 N. Bhardwaj, S. K. Bhardwaj, J. Mehta, M. K. Nayak and A. Deep, *New J. Chem.*, 2016, **40**, 8068–8073.
50 M. Rycenga, C. M. Cobley, J. Zeng, W. Li, C. H. Moran, Q. Zhang, D. Qin and Y. Xia, *Chem. Rev.*, 2011, **111**, 3669–3712.
51 J. Wu and C. Gao, *Macromol. Chem. Phys.*, 2009, **210**, 1697–1708.
52 L. T. Hoang, H. Van Pham and M. T. T. Nguyen, *J. Electron. Mater.*, 2020, **49**, 1864–1871.
53 N. La Ngoc Tran, D. Van Hoang, A. Tuan Thanh Pham, N. Tran Truc Phuong, N. Xuan Dat Mai, T. T. K. Chi, B. T. T. Hien, T. Bach Phan and N. H. T. Tran, *J. Sci.: Adv. Mater. Devices*, 2023, 100584.
54 J. Du and C. Jing, *J. Colloid Interface Sci.*, 2011, **358**, 54–61.
55 C. Li, Y. Huang, K. Lai, B. A. Rasco and Y. Fan, *Food Control*, 2016, **65**, 99–105.
56 S. W. Kang, Y. W. Lee, Y. Park, B. S. Choi, J. W. Hong, K. H. Park and S. W. Han, *ACS Nano*, 2013, **7**, 7945–7955.
57 Y. Cui, B. Li, H. He, W. Zhou, B. Chen and G. Qian, *Acc. Chem. Res.*, 2016, **49**, 483–493.
58 C. Zhang, B. Man, Z. Li, X. Xiu, L. Hou, J. Yu, S. Jiang, X. Zhao, Q. Peng, S. Qiu and C. Li, *Nanophotonics*, 2021, **10**, 1529–1540.
59 O. Guselnikova, P. Postnikov, R. Elashnikov, E. Miliutina, V. Svorcik and O. Lyutakov, *Anal. Chim. Acta*, 2019, **1068**, 70–79.
60 S. Mao, F. Pei, S. Feng, Q. Hao, P. Zhang, Z. Tong, X. Mu, W. Lei and B. Liu, *Colloids Surf., A*, 2023, **657**, 130595.
61 O. Nasr, Y. Y. Lin, Y. S. Chou, C. W. Huang, W. S. Chuang, S. W. Lee and C. Y. Chen, *Appl. Surf. Sci.*, 2022, **573**, 151509.
62 D. Papadakis, A. Diamantopoulou, P. A. Pantazopoulos, D. Palles, E. Sakellis, N. Boukos, N. Stefanou and V. Likodimos, *Nanoscale*, 2019, **11**, 21542–21553.
63 J. Yang, L. Zhou, X. Y. Wang, G. Song, L. J. You and J. M. Li, *Colloids Surf., A*, 2020, **584**, 124013.
64 E. C. Le Ru, E. Blackie, M. Meyer and P. G. Etchegoint, *J. Phys. Chem. C*, 2007, **111**, 13794–13803.
65 K. Wang, D. W. Sun, H. Pu, Q. Wei and L. Huang, *ACS Appl. Mater. Interfaces*, 2019, **11**, 29177–29186.
66 J. Li, X. Wang, G. Zhao, C. Chen, Z. Chai, A. Alsaedi, T. Hayat and X. Wang, *Chem. Soc. Rev.*, 2018, **47**, 2322–2356.
67 Y. Yang, J. Liu, Z. W. Fu and D. Qin, *J. Am. Chem. Soc.*, 2014, **136**, 8153–8156.
68 Q. Sun, Q. Y. Zhang, N. Zhou, L. Y. Zhang, Q. Hu and C. Y. Ma, *Appl. Surf. Sci.*, 2021, **565**, 150524.
69 S. Lin, R. Mandavkar, M. A. Habib, S. Burse, T. Khalid, M. H. Joni, M. Y. Li, S. Kunwar and J. Lee, *Appl. Surf. Sci.*, 2023, **611**, 155559.
70 N. La Ngoc Tran, D. Van Hoang, A. Tuan Thanh Pham, N. Tran Truc Phuong, N. Xuan Dat Mai, T. T. K. Chi, B. T. T. Hien, T. Bach Phan and N. H. T. Tran, *J. Sci.: Adv. Mater. Devices*, 2023, **8**, 100584.
71 M. Lafuente, S. De Marchi, M. Urbiztondo, I. Pastoriza-Santos, I. Pérez-Juste, J. Santamaría, R. Mallada and M. Pina, *ACS Sens.*, 2021, **6**, 2241–2251.